

B. SWITCHING CHARACTERISTICS OF NPT- AND PT-IGBTS UNDER ZERO-VOLTAGE SWITCHING CONDITIONS

B-I. INTRODUCTION

Recently, the demand for high voltage and high power IGBTs has been increasing. In order to achieve a device structure with high voltage blocking capability in the 1,200V range, the non-punch-through (NPT) type with non-buffer layer IGBT has become popular. Commercially available devices today in the 600 V range are mainly PT type, and in the 1,200 V range are mainly NPT type. These two device types behave differently in on-state voltage drop and dynamic switching because of their physical structure and carrier lifetime control. In a practical application circuit, the switching characteristics can be affected by parasitic components, temperature, and diode reverse recovery characteristics [1]-[2], [4], [8]-[11]. In general, the fundamental switching characteristics that are of concern in applications are: 1) di/dt and dv/dt device stresses, 2) turn-off tail current and switching energy, 3) high switching frequency capability, and 4) interaction with diode reverse recovery. Such fundamental characteristics can be changed with externally connected circuitry.

Recently, it was found that the IGBT switching characteristics were further influenced by external soft-switching circuitry [3]-[6]. However, different types of devices behave differently under soft-switching conditions. In a resonant snubber inverter (RSI) [3], the IGBT output is paralleled with an external snubber capacitor to reduce turn-off loss and turn-off dv/dt . This capacitor interacts with the output capacitance of the IGBT and affects the turn-off tail current magnitude and duration.

In this Appendix B, switching characteristics of NPT- and PT-IGBTs are evaluated under hard-switching and RSI based soft-switching conditions. Furthermore, the interaction between the external circuit and the IGBT internal model under ZVS operations is studied with various parameters.

B-II. IGBT TEST CIRCUIT WITH ZERO-VOLTAGE SWITCHING CONDITIONS

Fig. B-1 shows the IGBT test circuit for zero-voltage switchings [12]. The test circuit consists of a pair of switches (S_1 and S_2), a pair of diodes (D_1 and D_2), and one auxiliary switch. The two switches are synchronously conducting or blocking depending on the desired switching duties. Two diodes provide a freewheeling current path and a reverse voltage across the load to form a two-quadrant operation. Notice that the load current is unidirectional. When the load current is flowing in diodes D_1 and D_2 , turning on S_1 and S_2 would shut off the diode current, but on the other hand, produce a large diode reverse recovery current and turn-on loss. Snubber capacitors are added across the main devices to reduce turn off losses. The auxiliary branch is connected between the two phase-legs or across the load. This branch consists of one auxiliary switch, one fast recovery diode, and one resonant inductor.

In the test set-up, a small copper tube along with a toroidal current transformer (CT) is inserted between the IGBT terminal and the busbar for current measurements. The current on the secondary side of the CT is then monitored by a commercial CT that converts current to voltage for oscilloscope reading. The device voltage is simply monitored by a voltage probe. Fig. B-2 shows the operational key waveforms for the test circuit. The basic control is to turn on the auxiliary branch before turning on the main switch. The auxiliary branch takes over the current from the freewheeling diode and resonates with capacitors in parallel with the main switch. The main switch is turned on while the voltage across the main switch drops to zero after the resonant stage.

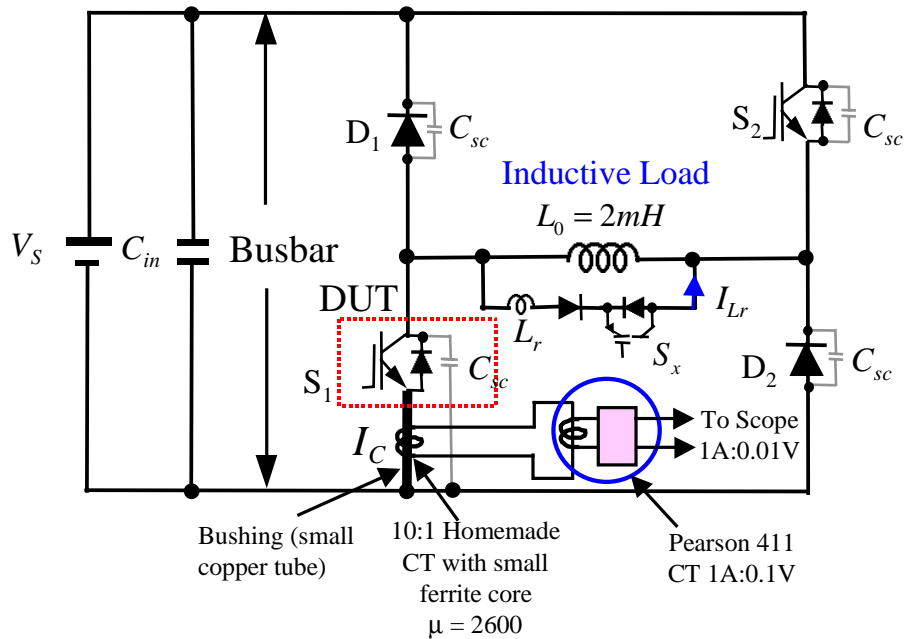


Fig. B-1. IGBT test circuit for zero-voltage switching.

Initially at t_0 , all switches are off, and the load current is freewheeling through D_1 and D_2 . Operational modes for a complete cycle are described in detail as follows.

Mode 0 ($t_0 - t_1$): Assume that load current is positive when D_1 and D_2 are conducting load current I_L , and main switches S_1 and S_2 are off.

Mode 1 ($t_1 - t_2$): Following the pulse-width-modulation (PWM) command, the auxiliary switch S_x turns on at t_1 , the auxiliary branch current I_{Lr} through the resonant inductor L_r increases linearly and the current in diode D_1 and D_2 decreases linearly. The auxiliary branch diverts the current from the freewheeling diode gradually.

Mode 2 ($t_2 - t_3$): After the auxiliary branch current is larger than the load current at t_2 , diodes D_1 and D_2 turn off naturally. Then all four snubber capacitors C_{sc} resonate with the L_r , and the voltage across the switch drops to zero in a finite dv/dt rate.

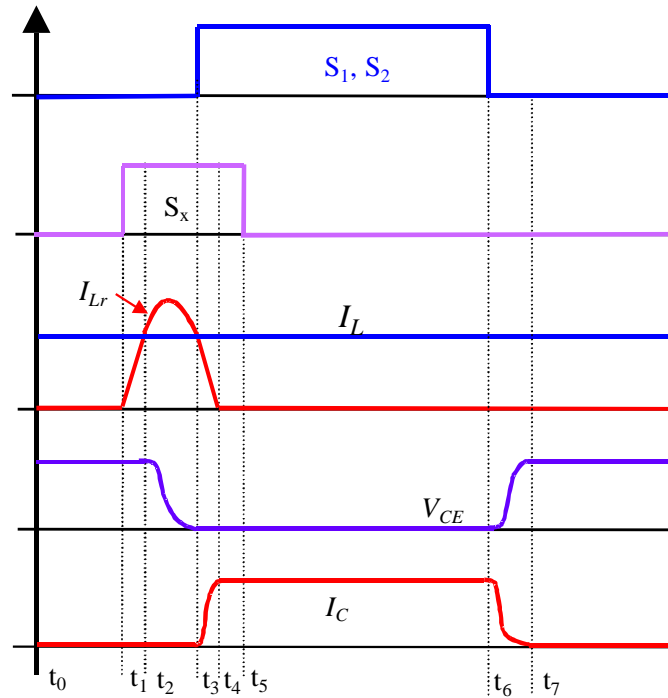


Fig. B-2. Operational key waveforms for zero-voltage switching.

Mode 3 ($t_3 - t_4$): At the end of the resonant stage, the snubber capacitors are discharged to zero voltage at t_3 . At this moment, the main switch can be turned on at zero-voltage condition. Since it is difficult to turn on the main switch at the exact moment capacitor voltage drops to zero without proper sensing, the main switch can only be turned on at a “near-zero-voltage” condition. After the main switches turn on, the inductor current decreases linearly due to reverse voltage polarity.

Mode 4 ($t_4 - t_5$): The resonant current decreases to zero at t_4 , and the auxiliary switch is turned off under zero-current condition at t_5 . The main switches conduct the load current, and the auxiliary switch and diode are both turned off after t_4 .

Mode 5 ($t_6 - t_7$): After the steady-state, ($t_5 - t_6$), main switches turn off losslessly with snubber capacitor. The I_L charges C_{sc} across S_1 and S_2 and discharges C_{sc} across D_1 and D_2 . The device voltage V_{CE} rises to the dc bus voltage, and the device current I_C drops to zero. Notice that the voltage rising rate is reduced by C_{sc} . After t_1 , the load current is completely freewheeling through D_1 and D_2 , and the operation returns to Mode 0.

B-III. IGBT PHYSICAL MODEL UNDER ZERO-VOLTAGE SWITCHING

In order to understand the IGBT operation under ZVS conditions, the physics-based circuit model is used to study the interaction between internal and external components. According to the test circuit in Fig. A-1, the external snubbing capacitor is added to the IGBT model for the ZVS circuit analysis. The external C_{sc} increases the output capacitance. This output capacitance interacts with internal circuit components of the IGBT, and turn-off characteristics are significantly changed. In this section, the IGBT model is combined with the added external snubber capacitor for the analysis of the NPT- and PT-IGBTs.

Fig. B-3 shows a schematic of the IGBT model combined with an external snubbing capacitor C_{sc} . With this snubbing capacitor added into the Saber IGBT model in [1]-[2], the total bipolar junction transistor (BJT) collector current I_c and the switching stage current I_t can be expressed as:

$$I_c = I_{css} + I_{ccer} \quad (\text{B-1a})$$

$$I_t = I_{sc} + I_c + I_b \quad (\text{B-1b})$$

where, I_{css} is the steady-state collector current, I_{ccer} is the collector redistribution current, I_{sc} is the snubbing capacitor current, and I_c and I_b are the collector and base current, respectively. The

steady-state collector current component of the BJT, I_{css} , is related to the non-quasi-static components in the base and charge-control components. Here, I_{css} is considered a controlled current source connected between the emitter and collector of the BJT.

The circuit interaction between the external capacitor, C_{sc} , and internal circuitry is discussed in the following observation. The redistribution current I_{cer} depends on the non-linear capacitor C_{cer} due to the moving base-collector boundary conditions, and the external snubbing capacitor current I_{sc} depends upon C_{sc} . These current components can be expressed as:

$$I_{cer} = C_{cer} \cdot \frac{dV_{CE}}{dt} \quad (\text{B-2a})$$

$$I_{sc} = C_{sc} \cdot \frac{dV_{CE}}{dt} \quad (\text{B-2b})$$

The difference in switching behavior between the NPT- and PT-IGBTs is due to the components of the collector-emitter redistribution capacitance C_{cer} that is dependent on the base width W of the PNP bipolar transistor. This W determines the effective output capacitance of the IGBT.

For an NPT-IGBT model, the C_{cer} in [1] is defined as:

$$C_{cer} = \frac{Q}{3Q_B} \cdot C_{bcj} \quad (\text{B-3a})$$

$$Q_B = qWN_B A \quad (\text{B-3b})$$

where Q is the excess carrier base charge, Q_B [1] is the background mobile carrier base charge, and C_{bcj} is the base-collector depletion capacitance. For high-level injection, Q is much larger than Q_B , and the redistribution capacitance is much larger than the depletion capacitance. Thus, Q dominates the output redistribution capacitance of the IGBT at turn-off. On the other hand, since Q is zero at the zero-current state before turn-on, the effective output capacitance is less important than that at turn-off.

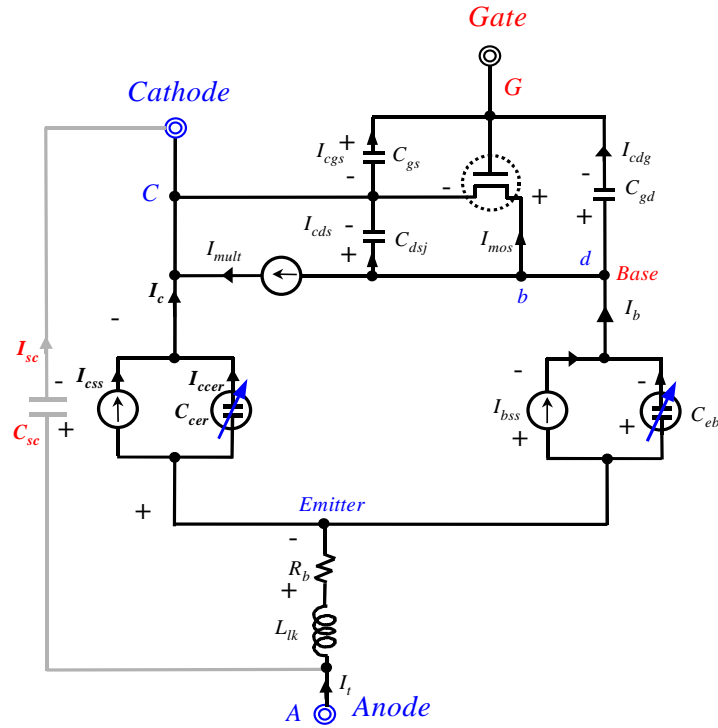


Fig. B-3. Physical IGBT model with an external snubbing capacitor.

The component of the collector current I_{css} is also governed by the charge Q , and thus it influences the turn-off characteristics. The expression for I_{css} [1] can be defined as

$$I_{css} \approx \frac{4D_p}{W^2} Q \quad (\text{B-4})$$

For a PT-IGBT model, the redistribution capacitance C_{cer} in [2] can be expressed as:

$$C_{cer} = \frac{W^2}{W_{eff}^2} \cdot \frac{Q}{Q_B} \cdot C_{bcj} \quad (\text{B-5})$$

where W is the width of the quasi-neutral low-doped base (LDB) region, and W_{eff} is the effective width for the base transport including the LDB and the buffer larger width.

As expressed in (B-5), the redistribution capacitance of a PT-IGBT model is dominated by the ratio W^2/W_{eff}^2 times Q/Q_B . Like an NPT-IGBT model, the influence of the base-collector depletion capacitance C_{bcj} is less important than that of the total redistribution capacitance. Because W is several times smaller for PT devices than for NPT devices and because $W^2/W_{eff}^2 < 1$, the ratio of I_{ccer} to I_{css} is much higher for the PT technology. This difference results in a difference in shape of the tail current bump between NPT and PT device types as describes in the next section.

B-IV. TURN-OFF CHARACTERISTICS

It is apparent that the experimental snubber capacitor alters the turn-off behavior significantly. However, the way the snubber capacitor produces a tail bump is not well understood. In order to explain the effects of the snubber capacitor, it is necessary to study the interaction between the snubber capacitor and the IGBT internal circuit model. The physics-based circuit model shown in Fig. B-3 is used for this study. The simulation for hard-switching condition is to verify the validity of the circuit model.

It was found from hardware experiments that IGBT turn-off current is significantly different in hard- and soft-switchings. Fig. B-4 (a) indicates that hard-switching turn-off dv/dt is approximately 2,000 V/ μ s, and the switching energy is almost 14 mJ at the load current of 200 A. With zero-voltage switching, as shown in Fig B-4 (b), dv/dt is reduced to 550 V/ μ s, and the turn-off switching loss is reduced from 14 to 8 mJ. It should be noticed that the PT-IGBT current tail in a zero-voltage switching condition is longer than in a hard-switching condition, and their shapes are also different. Under ZVS condition, the current tail exhibits a bump before it decays to zero, which did not occur in hard switching condition. Although the current tail duration in the soft-switching circuit is longer than that of the hard-switching circuit, the soft-switching circuit significantly reduces turn-off losses due to reduced slope of the voltage rising.

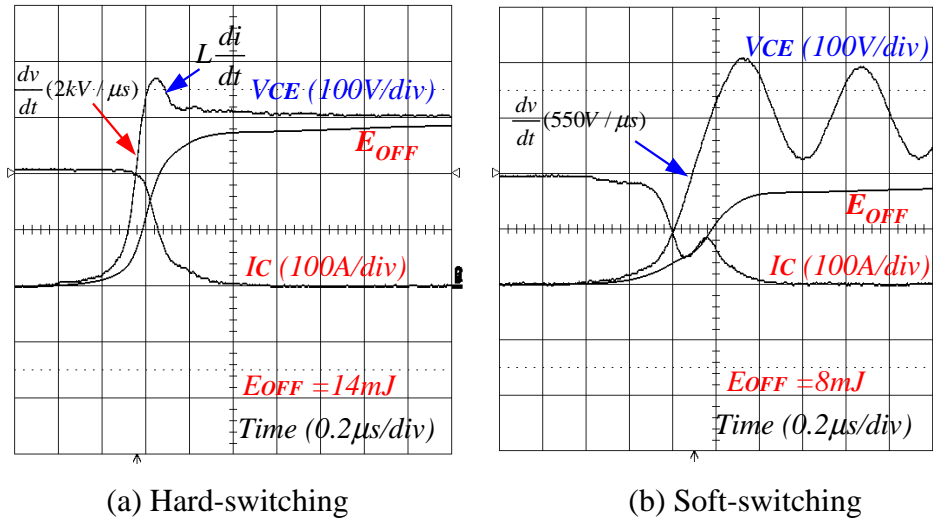


Fig. B-4. Experimental PT-IGBT turn-off switching waveforms under hard- and soft-switching with $0.1\mu\text{F}$ at 300 V bus and at 200 A.

Hard Switching

Fig. B-5 shows the simulated turn-off waveforms of the PT-IGBT under hard-switching condition. The simulation was done with the Saber circuit simulator. It can be seen that the simulated current and voltage match the experimental results very well. At a 200 A anode current condition, the MOSFET channel current, I_{mos} , shares 150 A, and the bipolar transistor collector current, I_c , shares 50 A in conduction state.

In this case, the bipolar transistor current burden is designed to be one-third the MOSFET current burden. This bipolar transistor burden strongly influences the turn-off tail current. Fig. B-5 illustrates the turn-off “tail” phenomena of the PT-IGBT collector current by a step-by-step.

$t_0 - t_1$: Assume that the IGBT is in its on-state with a gate bias. The turn-off voltage is applied to the gate of MOSFET in the IGBT to turn off the base current of the PNP bipolar transistor. The gate voltage V_{GE} slowly decreases exponentially with time due to the discharging of the gate capacitance via the gate series resistance.

- $t_1 - t_2$: At this stage, the gate drive voltage maintains the threshold voltage and starts to discharge gate-collector capacitance. When the device voltage V_{CE} starts to increase slowly, the MOSFET channel current I_{mos} begins to decrease slowly. The internal currents I_{css} and I_{ccer} of the bipolar transistor increase slowly at the same rate as the decay of I_{mos} .
- $t_2 - t_3$: The gate drive voltage continues to discharge the gate-collector capacitance. The device voltage V_{CE} rises to the dc bus voltage, and the IGBT collector current starts decreasing. During this stage, the MOSFET channel current I_{mos} decreases to zero. However, now the currents I_{css} and I_{ccer} increase while I_{mos} decays. The internal currents I_{css} and I_{ccer} have a peak value that maintains the total current nearly constant.
- $t_3 - t_4$: The gate voltage drops below the threshold voltage. The capacitor C_{cer} is charged to dc bus voltage, and the currents I_{css} and I_{ccer} are quickly diverted to the opposite side diode for freewheeling. Thus, I_{css} and I_{ccer} decrease with a high rate of current change, di/dt . This di/dt interacts with parasitic inductance and generates a voltage overshoot. As a result of the overshoot, a voltage fluctuation occurs that results in an increase of I_{ccer} , and thus the appearance of a tail bump.
- $t_4 \leq t$: The C_{cer} continues to create the tail bump as the voltage fluctuation diminishes. The tail current then exponentially approaches zero as the base charge and I_{css} decay.

Soft Switching

Fig. B-6 shows the PT-IGBT turn-off waveforms under the soft-switching condition with 0.1 μ F snubbing capacitor at 300 V bus and at 200 A. Turn-off characteristics under ZVS are analyzed as follows:

- $t_0 - t_1$: To cut off the base current of the PNP bipolar transistor, a negative voltage is applied to the gate of the internal MOSFET of the IGBT. As the gate voltage V_{GE} approaches the threshold voltage, I_{mos} decreases slowly. I_{css} and I_{ccer} of the bipolar transistor increase while I_{mos} declines to maintain the load current. As the collector

current voltage rises to provide I_{css} and I_{ccer} , the gate voltage remains constant as the gate-collector capacitance is discharged.

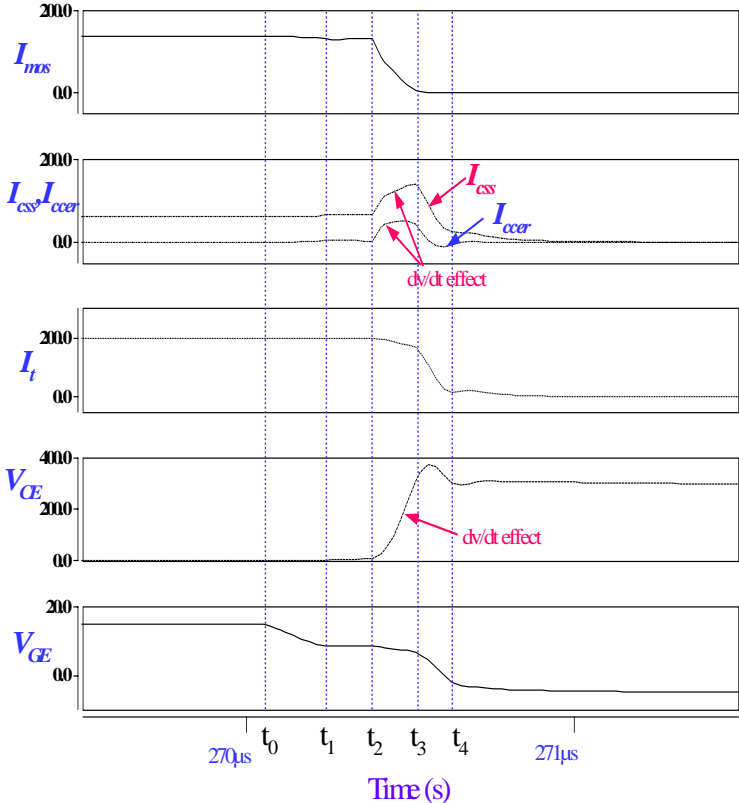


Fig. B-5. Simulated PT-IGBT turn-off switching waveforms under hard-switching at 300 V bus and at 200 A.

$t_1 - t_2$: When the gate drive voltage drops below the threshold voltage, the MOS channel current I_{mos} decreases exponentially to zero, the I_{sc} reaches its peak current, and the currents I_{css} and I_{ccer} increase a little and then begin to decrease. During this stage, the turn-off current tail remains invariant.

$t_2 - t_3$: The device voltage rises with a low dv/dt until the device voltage is clamped to dc bus voltage. The slow device voltage rising affects I_{css} and I_{ccer} . Since the device voltage is rising with a low dv/dt , the IGBT turn-off current slowly decrease and

thus generates “more tail bump” than hard switching where the clamped voltage is reached before the tail decay.

$t_3 - t_4$: During this stage, $I_{c\text{cer}}$ slowly reaches zero and the turn-off current tail bump decreases to zero at t_4 . However, the snubber capacitor resonates with the parasitic inductance, resulting in a significant oscillation in I_{sc} . This oscillation also appears in the collector voltage V_{CE} because of $L_{lk} \cdot (dI_{sc} / dt)$, where L_{lk} is the parasitic inductance on the power connection.

$t_4 \leq t$: When the device voltage is clamped to the dc bus voltage, the collector current is already turned off completely. The current in the snubber capacitor, however, continues to oscillate at a high frequency (5MHz in this case) due to the resonance between snubber capacitors and parasitic inductance.

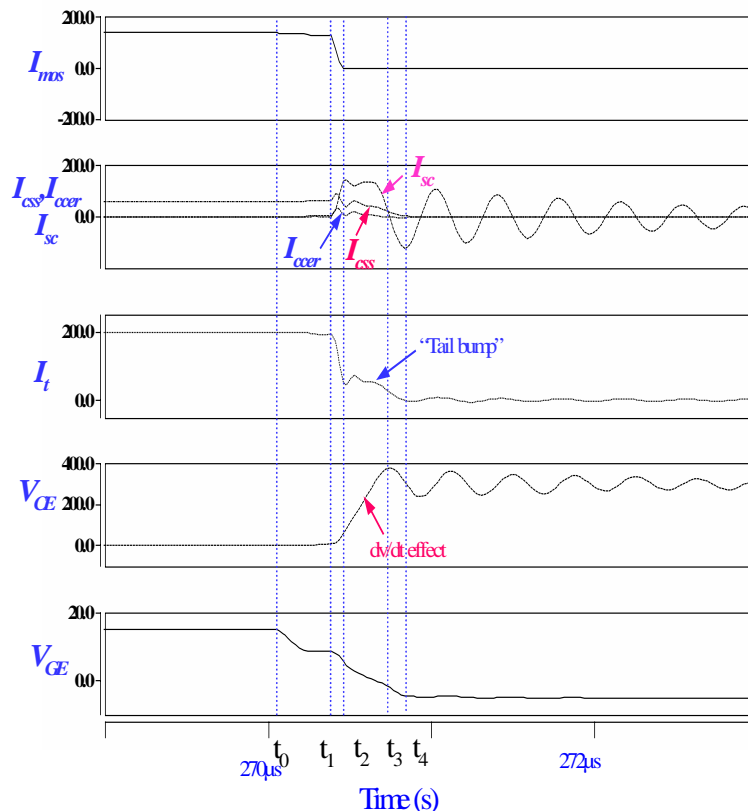


Fig. B-6. Simulated PT-IGBT turn-off switching waveforms under soft-switching with 0.1 μF at 300 V bus and at 200 A.

NPT Device

The NPT-IGBT switching behaviors are similar to that of the PT-IGBT. The difference is that the NPT-IGBT has a large redistribution output capacitance due to a wide drift region between the collector and emitter.

Fig. B-7 shows the experimental turn-off waveforms of the NPT-IGBT under hard- and soft-switching with a 0.14 μF snubbing capacitor at 630 V bus and 300 A. The turn-off tail current was observed to be like that of the PT-IGBT. As shown in Fig. B-7 (a), it is evident that the NPT-IGBT has a longer tail than that of the PT-IGBT due to the wide drift region in the base. Fig. B-7 (b) shows the experimental turn-off switching waveforms of the NPT-IGBT under soft-switching conditions. The soft-switching circuit achieved a reduction of dv/dt from 2,400 to 1,000 $\text{V}/\mu\text{s}$ and of the turn-off loss from 38 mJ to 18 mJ. Therefore, in both PT- and NPT-IGBTs, it can be concluded that the turn-off switching behaviors of the IGBT are influenced by the snubbing capacitor.

As shown in Fig. B-8, the turn-off waveforms under hard-and soft-switching conditions have been verified through the simulation. This simulation was done with the Pspice circuit simulator implementation of Hefner's NPT IGBT model that includes parameters of the IGBT. As a result, it can be seen that the simulated current and voltage match well the experimental results.

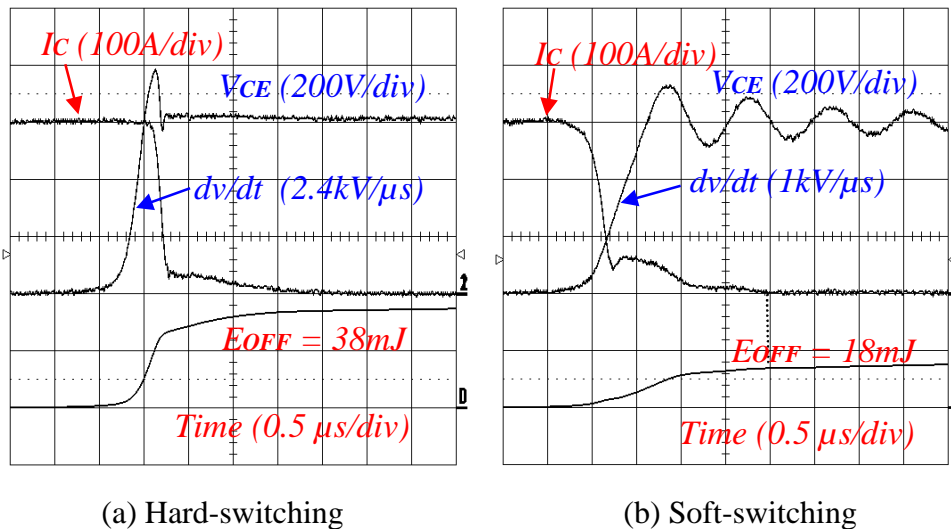


Fig. B-7. Experimental NPT-IGBT turn-off switching waveforms under hard- and soft-switching with 0.14 μF at 630 V bus and turn-off at 300A.

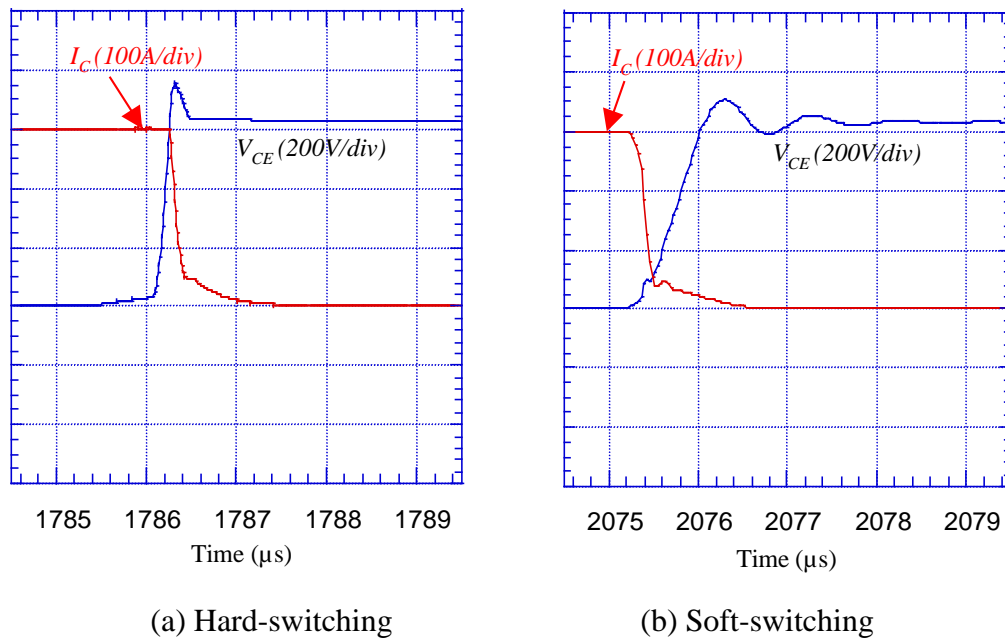


Fig. B-8. Simulated turn-off waveforms of the NPT- IGBT under hard- and soft-switching with 0.14 μF at 630 V bus and 300 A.

Fig. B-9 shows the NPT-IGBT turn-off waveforms under ZVS operation with a 0.14 μF snubbing capacitor at 630 V bus and at 300 A. The tail current bump related to the redistribution capacitance C_{cer} of the device was observed from the NPT-IGBT turn-off current. As expected, it was found that the ratio of I_{cer} to I_{css} is lesser than that of the PT-IGBT as shown in Fig. B-6.

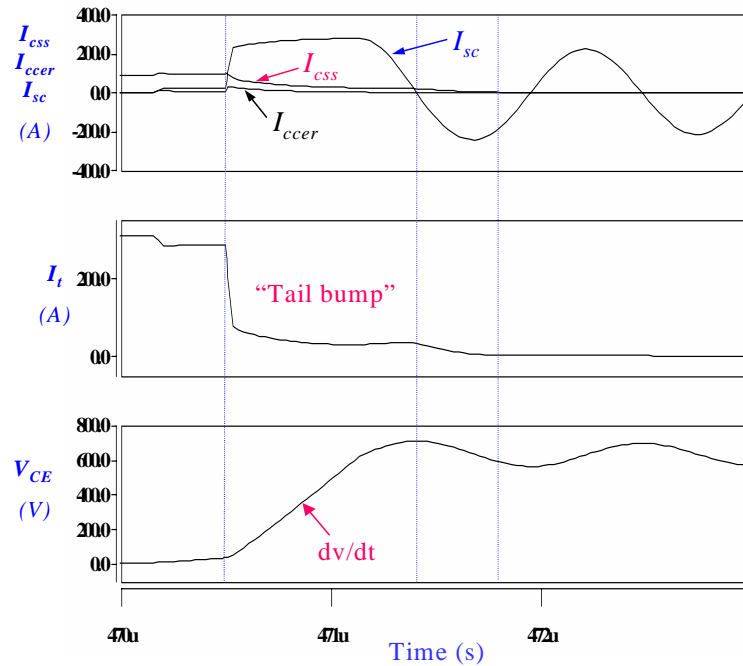


Fig. B-9. Simulated NPT-IGBT turn-off switching waveforms under soft-switching with $0.14 \mu\text{F}$ at 630 V bus and at 300 A.

B-V. TURN-ON CHARACTERISTICS

With snubber capacitors across the devices and the freewheeling diodes in the load current return path, the switch turn-on behavior is dominated by these external components. Fig. 10 illustrates the current direction of all the circuit devices and components during switch turn-on process. When switch S_1 turns on, diode D_1 must be turned off before the load current I_L can be diverted to S_1 . In hard-switching case, the total current flowing in S_1 can be expressed as

$$I_{S1} = I_L + I_{D1(rr)} + 2I_{sc} \quad (\text{B-6})$$

where $I_{D1(rr)}$ means the reverse recovery current of D_1 . However, the snubber capacitors C_{sc} 's are normally removed in most cases. The total switch current during turn-on can then be simplified as

$$I_{SI} = I_L + I_{DI(rr)} \quad (\text{B-7})$$

Fig. B-11 shows the experimental turn-on voltage, current, and energy waveforms of PT- and NPT-IGBTs without snubber capacitors. As can be seen from both current waveforms in Fig. B-10 (a) and (b), the peak current has an overshoot that is approximately 20% higher than the load current. According to (7), this overshoot can be attributed to $I_{DI(rr)}$.

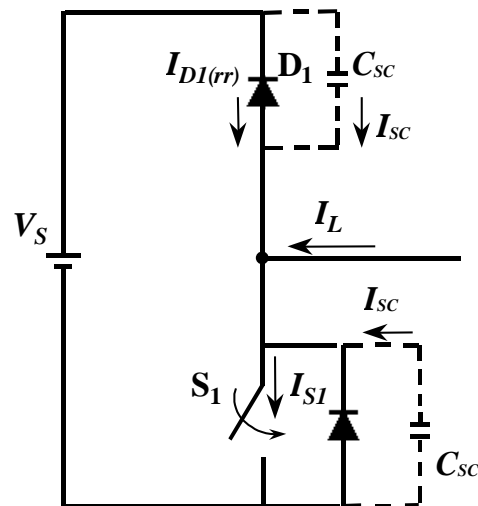


Fig. B-10. Switch turn-on condition in a typical converter circuit.

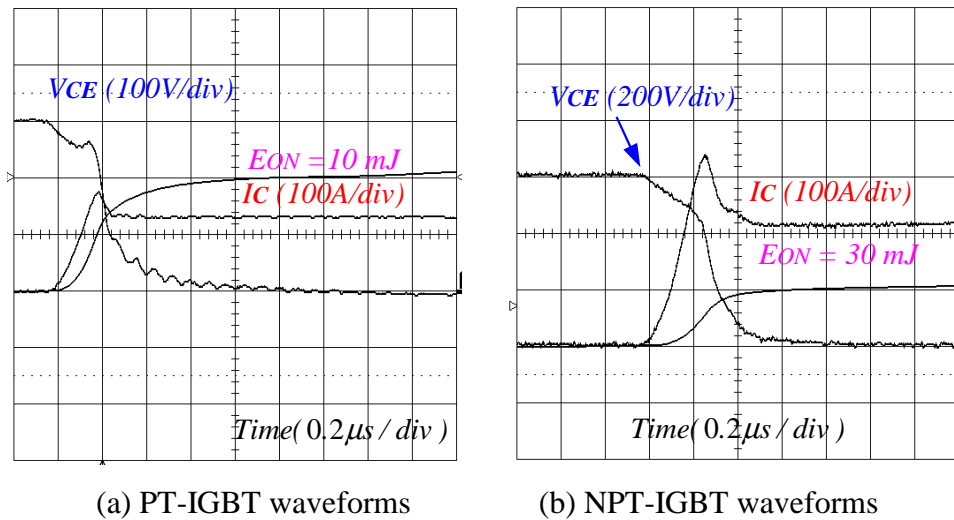


Fig. B-11. Experimental PT- and NPT-IGBT turn-on switching waveforms under hard-switching.

For the experimental condition shown in Fig. B-11 (a), the PT-IGBT is operating at 300 V, 130 A, and the turn-on energy is 10 mJ. For Fig. B-11 (b) condition, the NPT-IGBT is operating at 630 V, 220 A, and the turn-of energy is 30 mJ. The turn-on energy in both cases is not only affected by the turn-on characteristic of the IGBT switch S_1 , but also affected by the reverse recovery characteristic of the freewheeling diode D_1 .

With soft-switching operation, however, the total switch current is no longer affected by neither $I_{D1(rr)}$ nor by I_{sc} . As described in Fig. B-2, an auxiliary branch takes away the current from diode D_1 first, and the auxiliary resonant inductor L_r resonates with the snubber capacitor C_{sc} to divert the current into switch S_1 after the collector-emitter voltage V_{CE} drops to zero. The turn-on energy is practically eliminated in this case.

Fig. B-12 shows experimental turn-on voltage, current and energy for the NPT-IGBT under soft-switching condition. As explained in section II, the exact zero-voltage condition is difficult to achieve with the experimental chopper circuit. The turn-on condition in Fig. B-12 can only be considered as “near-zero-voltage” condition because the collector current I_C rises at the collector-emitter voltage V_{CE} near zero voltage condition. Although the true zero-voltage turn-on is not achieved in this case, the turn-on energy loss is reduced from 30 mJ to 1.5 mJ for the same dc bus voltage and load current condition.

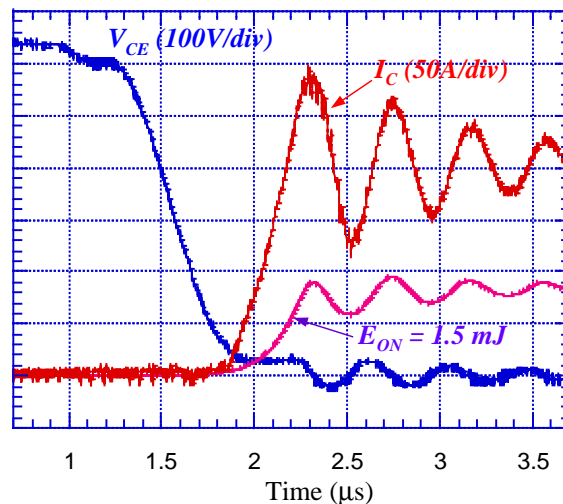


Fig. B-12. Experimental NPT-IGBT turn-on switching waveforms with $0.14 \mu\text{F}$ at 630 V bus and turn-on at 220 A

Similar to turn-off condition, the collector current oscillates during the process of transferring the load current into the switch because of the parasitic ringing. This parasitic ringing can be minimized with an elaborate layout and perhaps eliminated with removal of the current sensor.

From the discussion of Fig. 10 and experimental IGBT turn-on waveforms in Figures 11 and 12, it can be seen that the IGBT turn-on characteristic is dominated by the external components including freewheeling diodes and snubber capacitors. Significant turn-on loss reduction can be expected with the use of RSI based soft-switching circuit.

B-VI. CONCLUSION

In this Appendix-B, switching characteristics of PT- and NPT-IGBTs were evaluated under soft-switching conditions. The turn-off tail current characteristics were examined to study the interaction between the external circuit and the IGBT internal conduction mechanisms. In particular, the effects of an external circuit containing a snubber capacitor were studied. Both PT- and NPT-IGBTs exhibit a turn-off tail bump under ZVS operation. The major difference between these two devices is the redistribution capacitance, C_{cer} . The PT device has a larger ratio of I_{ccer} to I_{css} than that of the NPT device, resulting in a difference in shape of tail current bump.

The external components not only affect the IGBT turn-off behaviors, but also alter its turn-on characteristic. With the experimental auxiliary resonant snubber circuit, the diode reverse recovery current is no longer a factor during turn-on process, and the turn-on energy loss can be nearly eliminated.

The results of this study may help formulate guidelines to design the IGBT and to select the snubbing capacitor in soft-switching inverter and converter applications.

REFERENCES

- [1] A. R. Hefner, Jr., and D. M. Diebolt, "An Experimentally Verified IGBT Model Implemented in Saber Circuit Simulator," *IEEE Trans. on Power Electronics*, Vol. 9, No. 5, Sept. 1994, pp. 532-542.
- [2] A. R. Hefner, Jr., "Modeling buffer layer IGBT's for Circuit Simulation," *IEEE Trans. on Power Electronics*, Mar. 1995, pp. 111-123.
- [3] J. -S. Lai, "Fundamentals of a New Family of Auxiliary Resonant Snubber Inverters," *Conf. Rec. of IEEE IECON*, Nov. 1997, pp. 645-650.
- [4] S. Pendharkar, and K. Shenai, "Zero Voltage Switching Behavior of Punch Through and Nonpunch Through Insulated Gate Bipolar Transistors (IGBT's)," *IEEE Trans. on Electronic Devices*, Vol. 45, No. 8, August 1998, pp. 1826-1835.
- [5] I. Widjaja, K. Kunrnia, K. Shenai, and D. M. Divan, "Switching Dynamics of IGBT's in Soft-Switching Converter," *IEEE Trans. on Electronic Devices*, Vol. 42, No. 3, March 1995, pp. 445-454.
- [6] A. Elasser, M. J. Schutten, V. Vlatkovic, and D. A. Torrey, "A Study of Internal Device Dynamics of Punch-Through and Non Punch-Through IGBTs under Zero-Current Switching," *IEEE Trans. on Power Electronics*, Vol. 12, No. 1, January 1997, pp. 21-27.
- [7] R. Siesmience, M. Netzel, and R. Herzer, "Comparison of PT and NPT Cell Concept for 600V IGBTs," *Conf. Rec. of EPE'97*, 1997, pp. 4.024-4.028.
- [8] S. Azzoparadi, C. Jampt, J. -M. Vinnasa, and C. Zardini, " Switching Performances Comparison of 1200V Punch-Through and Non Punch-through IGBTs under Hard Switching at High Temperature," *Conf. Rec. of IEEE-PESC*, Jun 1998, pp. 1201-1207.
- [9] F. Blaabjerg, J. K. Pedersen, and U. Jaeger, "A Critical Evaluation of Modern IGBT-Modules," *Conf. Rec. of EPE'95*, 1995, pp. 1.594-1.601.
- [10] A. R. Hefner, Jr., " A Dynamic Electrothermal Model for the IGBT," *IEEE Trans. on Ind. Appl.* Mar. 1994, pp. 394-405.
- [11] B. J. Baliga, "Power Semiconductor Device," PWS Publishing Com., 1998.
- [12] B. M. Song, and J. S. Lai, " A Novel Two-Quadrant Soft-Switching Converter with One Auxiliary Switch for High Power Applications," *IEEE Trans. on Ind. Appl.*, Vol. 36, No. 5, 2000, pp. 1388-1395.